AIChE WILEY InterScience DISCOVER SOMETHING GREAT

PARTICLE TECHNOLOGY AND FLUIDIZATION

Steam Reactivation of a Spent Sorbent for Enhanced SO_2 Capture in FBC

Fabio Montagnaro
Dipartimento di Chimica, Università degli Studi di Napoli Federico II, Complesso Universitario del Monte di Sant'Angelo, 80126 Napoli, Italy

Fabio Pallonetto and Piero Salatino
Dipartimento di Ingegneria Chimica, Università degli Studi di Napoli Federico II, Piazzale Vincenzo Tecchio 80, 80125 Napoli, Italy

Fabrizio Scala
Istituto di Ricerche sulla Combustione, Consiglio Nazionale delle Ricerche, Piazzale Vincenzo Tecchio 80, 80125 Napoli, Italy

DOI 10.1002/aic.11026
Published online October 30, 2006 in Wiley InterScience (www.interscience.wiley.com).

The regeneration by steam hydration of the sulfur capture ability of spent sorbent particles from Fluidized Bed Combustion (FBC) is addressed. The process is characterized in terms of effectiveness of sorbent reactivation, hydration degree, particle sulfation pattern, development of accessible porosity, and extent of particle attrition and fragmentation. Steam reactivation experiments were carried out in a lab-scale atmospheric FBC at 250°C for 10, 30, and 180 min with 0.05 MPa steam partial pressure. The effectiveness of sorbent reactivation was assessed by reinjecting the reactivated material into the FB reactor operated at 850°C under simulated desulfurization conditions and following the degree of calcium conversion and the attrition rate along with resulfation. The experimental results indicated that steam reactivation is effective in renewing the SO_2 uptake ability of the exhausted sorbent particles. The regeneration mechanism based on the swelling upon hydration of the unreacted core, the generation of fissures and cracks, and the consequent development of accessible porosity is confirmed for the limestone under scrutiny. In addition to this, a remarkable result was that steam hydration induces, for the sorbent under investigation, a pronounced sulfur redistribution throughout the particle cross-section, which provides another pathway to the enhancement of the sulfur capture ability of the reactivated sorbent. © 2006 American Institute of Chemical Engineers *AIChE J,* 52: 4090–4098, 2006
Keywords: fluidized bed combustion, sulfur capture, steam reactivation, fragmentation, attrition

Introduction

The possibility of achieving in situ removal of SO_2 by the injection of a calcium-based sorbent in a Fluidized Bed Combustor (FBC) is attractive, since limestone is relatively cheap and displays peak sulfur capture efficiencies around the typical range of FBC operating temperatures.[1,2] Sorbent sulfation has been investigated in detail in the past[3–9] and, under over-

Correspondence concerning this article should be addressed to F. Montagnaro at fabio.montagnaro@unina.it.

all oxidizing conditions and at atmospheric pressure, proceeds according to the following reactions:

$$CaCO_3\ (s) \Leftrightarrow CaO\ (s) + CO_2\ (g) \quad (1)$$

$$CaO\ (s) + SO_2\ (g) + \frac{1}{2}O_2\ (g) \Leftrightarrow CaSO_4\ (s) \quad (2)$$

Microscopic investigation of spent particle cross-sections revealed that limestones of different origin may undergo a variety of sulfation patterns: i) *core/shell* sulfation pattern, characterized by the formation of a $CaSO_4$-rich outer shell, which prevents further sulfation of the unreacted core; ii) *network* sulfation pattern, in which fractures/cavities typical of the original particle texture favor the formation of multiple unreacted CaO nuclei surrounded by sulfated layers; iii) *uniform* sulfation pattern, where the clear-cut distinction between unsulfated and sulfated zones throughout the particles is lost. The relationships existing among the properties of the native limestone, the process conditions, and the ultimate sulfation pattern have not been completely clarified and are the subject of considerable research effort.[4,5]

To complete the mechanistic framework of sorbent conversion in FBC, it should be recalled that substantial changes in size distribution of sorbent particles can be brought about by particle fragmentation and attrition.[10–14] *Primary fragmentation* occurs immediately after sorbent feeding, driven by thermal stresses and by internal overpressure associated with the course of calcination. Primary fragmentation, sometimes referred to as *decrepitation*, ends up with the generation of either coarse or fine fragments. *Attrition by abrasion* is determined by surface wear between sorbent particles and bed solids, and typically yields fine and quickly elutriable fragments. *Secondary fragmentation* of sorbent particles is most often associated with impact loading, yielding mostly coarse non-elutriable fragments. Both attrition by abrasion and secondary fragmentation are significantly affected by the parallel course of calcination and sulfation. In particular, the build-up of a hard sulfated shell in the core-shell or network sulfation patterns is responsible, in the long term, for the decrease of attrition and secondary fragmentation of sorbent particles.

FB combustion generates larger quantities of solid residues with respect to suspension firing. Moreover, these wastes are of worse quality when a possible re-use in the cement and concrete industry is considered.[15] This has driven research toward processes aimed at reactivating the spent sorbent, to limit ash disposal and sorbent consumption. Currently, sorbent reactivation by either water or steam hydration is receiving renewed consideration,[16–25] as demonstrated by the recently-built 790 MWth circulating FBC owned by ENEL and located in Sulcis (Sardinia, Italy), the first commercial unit designed to employ steam reactivation.[26]

The renewal of the SO_2 sorption ability of an exhausted sorbent as it is reactivated by water or steam has been related to the formation of $Ca(OH)_2$ as unreacted CaO is hydrated. The larger molar volume of calcium hydroxide with respect to calcium oxide determines the swelling of the core of hydrated particles and the subsequent breakage of their sulfated shells. This process enhances further exploitation of the sulfur capture ability of the reactivated particles, as they are reinjected into the combustor. In addition to this mechanism, recent studies on the liquid-phase hydration of a spent sorbent highlighted the occurrence of a pronounced sulfur redistribution throughout the sorbent particles. Since this process, which further contributes to the enhancement of the reactivation-induced sulfur uptake,[19,23] has not been observed with other spent sorbents,[27] it remains to be clarified whether sulfur redistribution is a general or sorbent-specific process and what factors could promote it.

It is the subject of considerable debate whether the core/shell or network sulfation patterns are essential prerequisites for hydration-induced reactivation to be effective. The susceptibility of some uniformly sulfating limestones to be effectively reactivated by hydration has been recently demonstrated,[28] at odds with previously reported findings.[4] When considering this much-debated subject, one should bear in mind that the very distinction between network and uniform sulfation patterns presents some degree of arbitrariness. In fact, the distinction between the heterogeneous and the homogeneous nature of a spent limestone, through the recognition of reacted/unreacted domains within the particle, is crucially related to the space-resolution with which the fine structure of the limestone is probed by SEM-EDX analysis of particle cross-sections. This space-resolution is seldom reported in previously published studies, thus preventing the possibility of a definitive assessment of whether particle heterogeneities might be obscured by lack of resolution. Altogether, it appears that the lack of characterization of petrographic and microtextural properties of limestones, either unreacted or preprocessed, somewhat undermines the possibility to make reliable predictions about the sulfation and reactivation patterns for limestones of different origin and nature.

Consideration of the effect of fuel ash on reactivation of spent sorbent further complicates the matter. Reactivation by water hydration of industrial FBC ashes generates, besides $Ca(OH)_2$, several calcium silico/sulpho/aluminate hydrates, like ettringite[29–31]; the formation of these binding phases, which can be exploited for further desulfurization, may on the other hand adversely influence the operation of regenerators by promoting agglomeration of hydrated particles. Careful design and operation of the regenerator is, therefore, required to overcome operational issues.[32] Conversely, the formation of a dry product and the limited fraction of binding phases after steam reactivation of spent FBC ashes makes it possible to overcome agglomeration. When comparing steam- and water-reactivation, it must be considered that intraparticle diffusion across the sulfate shell may limit the effectiveness of steam/CaO contact, making sorbent reactivation slower. This phenomenon is not generally encountered in water reactivation, as H_2O permeates the shell of the spent sorbent particles by capillary penetration.

The proper choice of reactivation temperature is also subject to debate. Water hydration is usually favored by higher temperatures. On the other hand, the optimal steam reactivation temperature is established by considering the competition between intraparticle diffusion and chemical reaction. At high temperatures, the chemical reaction ceases to be the rate-limiting step, and steam, diffusing toward the CaO grains, reacts rapidly at their surface, filling intraparticle voids; this may yield a "double-layer structure" (an external layer of $CaSO_4$ and an internal layer of $Ca(OH)_2$), which covers the unhydrated CaO core and hampers further hydration. Conversely, at lower temperatures, both diffusion and

chemical reaction are rate-controlling, thus favoring a more uniform hydration of unreacted CaO. Altogether, the combined effect of the process temperature on surface area, porosity, and pore size distribution of the reactivated sorbents has been observed,[20] indicating the existence of an optimum reactivation temperature around 300°C. Finally, the need to keep the reactivation temperature as high as possible should be borne in mind, to avoid heat losses associated with cooling and reheating ashes.

The present work addresses the steam reactivation of an Italian limestone. The influence of the hydration time on the extent of steam reactivation is assessed. The changes of microstructural and morphological properties of the reactivated sorbents are characterized and related to the corresponding renewal of the SO_2 uptake ability. The analysis is pursued further to the characterization of the influence of steam hydration on the fragmentation and attrition propensity of the regenerated sorbent.

Experimental

Materials

Sulfated (S), steam hydrated (H), dehydrated (D), and resulfated (RS) samples were obtained from the raw sorbent (R) through the following steps:

$$\mathrm{R} \xrightarrow{\text{calcination \& first sulfation}} \mathrm{S} \xrightarrow{\text{steam hydration}} \mathrm{H} \quad \begin{cases} \xrightarrow{\text{dehydration}} \mathrm{D} \\ \xrightarrow{\text{resulfation}} \mathrm{RS} \end{cases} \tag{3}$$

The raw sorbent was an Italian high-calcium (96.8% $CaCO_3$) limestone, commercially referred to as Massicci.

Gases used in the different tests were N_2 (supplied in cylinders), steam (from vaporization of distilled water), SO_2-N_2 mixtures (0.3% SO_2, supplied in cylinders) and technical grade dehumidified air. In addition to the raw or pre-processed sorbent samples, the bed in all FB but H tests consisted of silica sand.

Apparatus: the fluidized bed converter

Experimental tests were carried out in a stainless steel atmospheric bubbling FB reactor (Figure 1). The reactor is a laboratory-scale facility, 40 mm ID, consisting of three sections: a) the preheater/premixer of the fluidizing gas (height = 0.66 m) at the bottom; b) the fluidization column (height = 0.95 m); c) the two-exit head, made of brass and mounted on top of the fluidization column, to which the solids feeding hopper and exhaust line are connected. A 3 mm-thick perforated plate (49 holes of 0.5 mm ID in a triangular pitch) serves as gas distributor.

The reactor is electrically heated by two semi cylindrical ovens (2.4 kW each, 0.60 m-height, OD = 0.22 m) located around the upper part of the preheater/premixer and the lower part of the fluidization column. Heat losses from the ovens are limited by ceramic fiber insulation. A type-K thermocouple measures the temperature at 40 mm above the gas distributor, flush to the inner surface of the fluidization column. The thermocouple is connected with a PID temperature controller modulating electrical power supply to the ovens. The upper part of the fluidization column is unlagged so as to favor rapid cooling down of gases and prevent further reactions of elutriated fines.

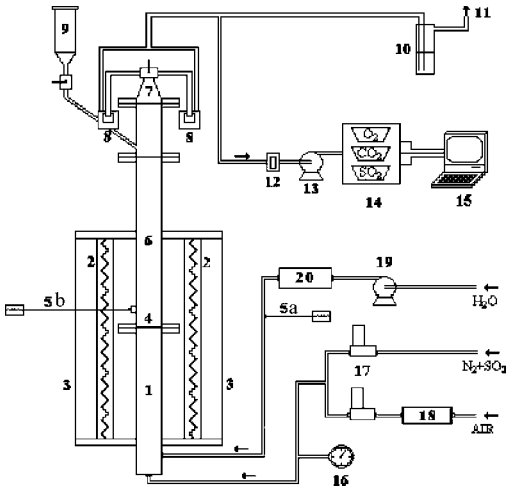

Figure 1. Sketch of the FB reactor employed.

1 = gas preheating/premixing section; 2 = electrical furnaces; 3 = ceramic insulators; 4 = gas distributor; 5a = thermocouple; 5b = thermocouple connected to a PID temperature controller; 6 = fluidization column; 7 = head with three-way valve; 8 = sintered brass filters; 9 = hopper; 10 = SO_2 scrubber; 11 = stack; 12 = cellulose filter; 13 = membrane pump; 14 = gas analyzers; 15 = personal computer; 16 = manometer; 17 = digital mass flow meters/controllers; 18 = air dehumidifier (silica gel); 19 = peristaltic pump; 20 = vaporizer.

Nitrogen, air, and the SO_2-N_2 mixture are supplied to the reactor by means of mass flow meters/controllers (Brooks, 0154/5850). Steam is generated by a specially designed water vaporizer, made of a ceramic tubular pipe wrapped by electric resistances and insulated by ceramic fiber. The electric resistances are connected to a variable voltage electrical supply in order to modulate the heat transferred to the distilled water, fed to the vaporizer by a peristaltic pump (Stepdos, FEM 03.18 RC). A thermocouple measures the temperature of the generated steam, which is fed to the preheater/premixer section immediately below the electrical ovens to avoid steam condensation.

The two-exit head is purposely designed to convey flue gases through either of two 25 mm ID cylindrical sintered brass filters (height = 35 mm, filtration efficiency = 1 for >10 μm-particles). Alternated use of filters enables time-resolved capture of elutriated fines at the exhaust. On-line analysis of flue gas is accomplished. In particular, SO_2 is detected by nondispersive infrared analyzer (Hartmann & Braun, Uras 3G), whose precision and reproducibility is better than $\pm 5\times10^{-3}$%. Concentration signals are logged on a PC at a sampling rate of 1 Hz.

Procedures: first sulfation (S) and resulfation (RS) of sorbent samples

The operating conditions of S and RS tests are reported in Table 1. Sorbent (either R or H) particles were sieved in the size range 0.4-0.6 mm and sulfated at 850°C by fluidizing the FB reactor at 0.8 m/s with an SO_2-O_2-N_2 mixture (0.18% SO_2, 8.5% O_2). The bed consisted of 20-25 g of sorbent + 150 g of 0.85-1 mm silica sand (this coarser size range was chosen

Table 1. Operating Conditions for Sulfation (S), Steam Hydration (H), Dehydration (D), and Resulfation (RS) Tests

	S	H	D	RS
Bed material	raw sorbent (20 g) + sand (150 g)	exhausted sorbent (50 g)	reactivated sorbent (15 g) + sand (150 g)	reactivated sorbent (25 g) + sand (150 g)
Sorbent size range	0.4-0.6 mm	0.4-0.6 mm	0.4-0.6 mm	0.4-0.6 mm
Sand size range	0.85-1 mm	–	0.85-1 mm	0.85-1 mm
Temperature	850°C	250°C	850°C	850°C
Time	180 min	10, 30 and 180 min	5 min	180 min
Gas inlet composition	0.18% SO_2–8.5% O_2-N_2	50% N_2–50% steam	air	0.18% SO_2–8.5% O_2-N_2
Gas superficial velocity	0.8 m/s	0.2 m/s	0.8 m/s	0.8 m/s

so as to easily separate the two solids by gentle sieving after the tests). The tests lasted 180 min, and the degree of calcium conversion was calculated as a function of time by working out the SO_2 concentration at the exhaust according to:

$$X_{Ca}(t) = \frac{\int_0^t \left[F_{SO_2}^{in} - F_{SO_2}^{out}(t)\right] dt}{n_{Ca}} \quad (4)$$

where $F_{SO_2}^{in}$ and $F_{SO_2}^{out}(t)$ are, respectively, the molar rates of SO_2 fed to the reactor and at the exhaust, and n_{Ca} are the moles of calcium in the raw sorbent initially fed to the reactor (see Eqs. 1 and 2). Strictly speaking, this value is influenced by the loss of CaO in the elutriated fines, which is appreciable at the beginning of the sulfation test; this was taken into account by estimating the loss of unconverted calcium in the elutriated fines throughout the test. $X_{Ca}(t)$ was reproducible within $X_{Ca}(t) \pm 1\%$. SO_3 concentration at the exhaust was not monitored, but it was accounted for when processing SO_2 concentration.[10] The specific elutriation rate of fines E(t) was calculated as the mass of elutriated fines collected in the filter per unit time and per unit initial mass of sorbent. Moreover, R and S particles were analyzed by mercury porosimetry, and S samples by SEM-EDX.

Procedures: steam hydration-reactivation (H) of spent sorbent

The operating conditions of the experimental tests are reported in Table 1. Exhausted (S) sorbent particles were reactivated by steam hydration in the FB reactor, at 250°C. Hydration times (t_H) investigated were $t_H = 10$, 30, and 180 min. The reactor was charged with a bed of 50 g of spent sorbent (particle size range = 0.4-0.6 mm), subsequently fluidized at 0.2 m/s with a steam-N_2 (50%-50%) gas mixture. At the end of the tests, the bed was discharged and H particles were analyzed by XRD and SEM-EDX. Moreover, the effect of the H treatment on the fragmentation of sorbent particles was assessed by sieving (in 9 size ranges between 0 and 0.6 mm), after the tests, the bed material in order to obtain the particle size distribution and the mean Sauter diameter:

$$d_S = \frac{1}{\sum_i x_i/d_i} \quad (5)$$

where x_i is the mass fraction of the particles having mean diameter d_i.

Procedures: dehydration (D) of reactivated sorbent

H particles were sieved in the size range 0.4-0.6 mm and dehydrated for 5 min at 850°C by fluidizing the FB reactor with air at 0.8 m/s (see Table 1). In D tests the bed consisted of 15 g of reactivated sorbent + 150 g of 0.85-1 mm silica sand. At the end of the experiments, the bed was discharged and D particles were analyzed by mercury porosimetry. In addition, the effect of the D treatment on the fragmentation of sorbent particles was assessed by sieving the bed material after the tests in order to obtain the particle size distribution and the mean Sauter diameter.

Microstructural characterization: SEM-EDX analysis

Particle cross-sections of S and H material (polished and embedded in epoxy resin) were analyzed at magnification = 50× by means of a Scanning Electron Microscope (SEM)—Philips, XL30—with an LaB_6 filament and equipped with an Energy Dispersive X-ray (EDX) probe—Edax, DX-4, resolution = 138 eV—for elemental mapping of sulfur throughout the particle cross-section.

Microstructural characterization: CCSEM-EDX mapping technique

An algorithm was purposely set up for automated analysis of EDX elemental maps with the aim of obtaining semi-quantitative indicators of sulfur distribution throughout the particle cross-section.[33] This Computer Controlled SEM-EDX (CCSEM-EDX) procedure, worked out in G programming language (National Instruments, IMAQ Vision), generates probability density functions of pointwise sulfur contents, which can be directly related to the sorbent particle sulfation pattern.

A Relative Sulfur Content (RSC) is defined as the intensity of the signal generated by the EDX sulfur map (varying from 0 to 2^8). The RSC value obtained by the mapping procedure could not be quantitatively related to the actual local sulfur content. However, since it was obtained according to a strictly reproducible and standardized protocol, it provided a reliable tool for semi-quantitative comparative analysis of samples of different nature. Figure 2 exemplifies the interpretation of RSC plots: a) Bimodal probability density functions of sulfur content are indicative of core-shell or network particle sulfation patterns. In fact, one peak corresponds to the low-sulfur-content zone (core zone in the core-shell pattern, unreacted nuclei in the network pattern), another peak corresponds to the high-sulfur-content zone (shell zone in the core-shell pattern, sulfated grains in the network pattern); b) Unimodal distribution functions correspond to a uniform sulfur distribution throughout the particle.

Microstructural characterization: XRD analysis

H particles were characterized by X-Ray Diffraction (XRD, Philips, PW1710). XRD aimed at the qualitative spe-

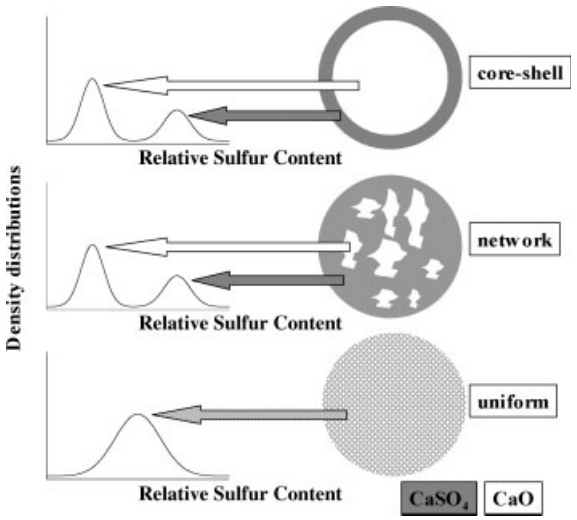

Figure 2. Assessment of sorbent sulfation patterns from probability density functions of relative sulfur content.

ciation of the main crystalline phases in hydrated-reactivated samples. The diffraction angle ranged from 5 to 60°2θ (Cu-Kα) with a 0.02°2θ increment.

Microstructural characterization: porosimetric analysis

Mercury porosimetry of R, S, and D samples was carried out by means of a porosimeter (Carlo Erba, P2000) operated at pressures ranging from 0.1 to 200 MPa (corresponding to pore radii in the range from 6800 to 4 nm). Porosimetric data were worked out in terms of cumulative pore undersize distributions.

Results

First sulfation (S) of raw sorbent

Figure 3 reports the degree of calcium conversion X_{Ca} as a function of time during first sulfation (S) tests. Operating conditions were such that the reactor could not be considered differential with respect to SO_2. In fact, SO_2 dropped to vanishingly small values at the beginning of the test, to increase thereafter until the inlet concentration was approached in the long term. This feature prevented the assessment of the kinetics of sulfur capture from differential analysis of X_{Ca} versus t curves. The ultimate degree of calcium conversion of the raw sorbent was 28%, a value consistent with published values for limestones of similar properties.[34]

Figure 4 reports the sorbent elutriation rate E(t) measured during S test. A pronounced spike was recorded at the beginning, followed by a monotonic decay of E(t) along the test. This trend results from the interplay of the following processes[10,11]:

(i) calcination brings about primary fragmentation into elutriable particles and coarse non-elutriable angular fragments;

(ii) removal of surface asperities (rounding off) from angular coarse fragments is extensive in the early stages of sorbent processing in FB, to decrease thereafter;

(iii) the progress of sulfation further reduces attrition and elutriation by strengthening the particle outer layer.

Results of porosimetric analysis on R and S samples are reported in Figure 5 and Table 2. For the sake of simplicity, pores with radius less than 100 nm will be referred to as "finer pores" hereinafter.[35] While the raw sorbent was relatively non-porous (porosity = 9%, cumulative specific pore volume = 34 mm^3/g), the spent sorbent showed relatively larger pore volumes (19% and 85 mm^3/g, respectively), as a consequence of the combined effect of full calcination (Eq. 1) and partial sulfation (Eq. 2) of the raw sorbent. The contribution of finer pores increased from 32% in the raw sorbent to 51% in the spent material.

The analysis of the morphological/textural changes associated with sulfation is completed by the SEM-EDX characterization of the cross-section of an S multiparticle sample, reported in Figure 6. Inspection of this figure reveals that particles are prevailingly sulfated according to core-shell and network patterns, though a few uniformly sulfated particles could also be detected. This was quantitatively confirmed by CCSEM-EDX (Figure 7 and Table 3), where a bimodal distribution function (typical of core-shell and network sulfation patterns, Figure 2) was obtained, featuring a core-zone area = 35%.

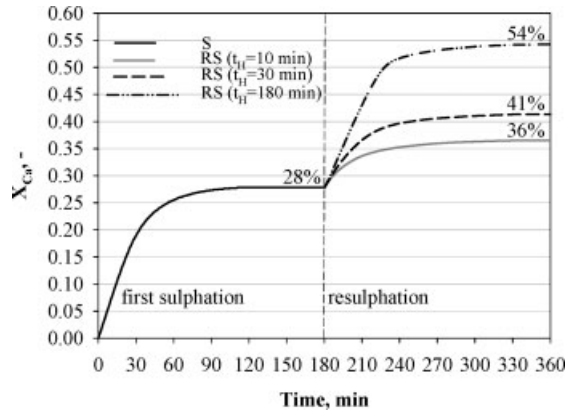

Figure 3. Degree of calcium conversion as a function of time during S and RS tests.

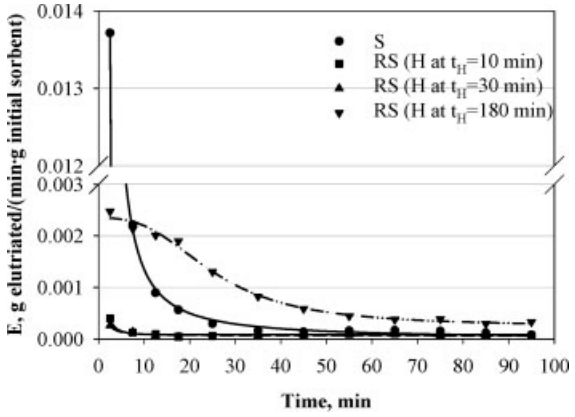

Figure 4. Specific fines elutriation rate during S and RS tests.

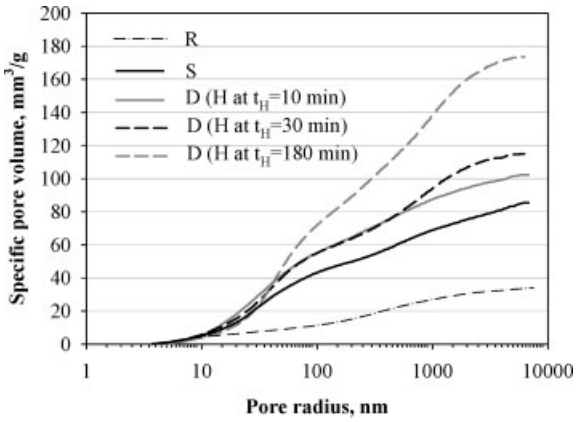

Figure 5. Cumulative pore undersize distribution of R, S, and D samples.

Steam hydration-reactivation (H) of spent sorbent

Figure 8 reports the XRD spectra for steam hydrated-reactivated (H) samples. At all t_H investigated it can be observed that $CaSO_4$ does not give rise to any gypsum-like phase. For $t_H = 10$ and 30 min, the course of the hydration reaction ($CaO \Rightarrow Ca(OH)_2$) determines a higher intensity of portlandite peaks, while the level of lime peaks correspondingly decreases. Hydration is completed only after $t_H = 180$ min, where lime peaks cannot be observed any more. Quartz peaks appearing in the spectra are to be related to small sand impurities.

Figure 9 shows the particle size distribution of the H samples. Hydration times of 10 and 30 min do not induce significant particle fragmentation; in both cases, less than 8% of the particles are found in the range 0-0.4 mm, and the occurrence of particles in the range 0-0.1 mm is negligible. Consequently, the Sauter mean diameter d_S (0.47 mm) is very close to that of the feeding. By contrast, at $t_H = 180$ min the hydration-induced fragmentation is much more pronounced: 51% of the particles fall in the range 0-0.4 mm, and a non-negligible fraction of particles fall in the range 0-0.1 mm; correspondingly, d_S is much smaller (0.22 mm). This result should be related to the prolonged stay of the particles in the FB reactor at $t_H = 180$ min and to the complete hydration-induced swelling effect.

Figure 6 reports the SEM-EDX mapping of H multiparticle sample cross-sections. It can be recognized that the longer t_H, the larger the fraction of uniformly sulfated particles. This finding suggests that the steam hydration-reactivation treatment promotes sulfur redistribution from the shell zone to the core zone, resulting in a larger extent of unsulfated calcium in the shell—available for resulfation—as compared with the spent sorbent. The occurrence of sulfur redistribution was recently reported for the first time[19,23] as resulting from the water-hydration of the same limestone employed in the present study. In that case, sulfur redistribution was explained in the light of a solubilization/precipitation mechanism involving ionic species via the aqueous phase. It could be speculated that similar redistribution processes, potentially promoted by the presence of adsorbates, might be at work during steam hydration. Further work is needed to fully elucidate the mechanisms responsible for redistribution.

Table 2. Results of Porosimetric Analysis

Sample	Porosity	Cumulative Specific Pore Volume	Fraction of Finer Pores
R	9%	34 mm^3/g	32%
S	19%	85 mm^3/g	51%
D (H at $t_H = 10$ min)	22%	102 mm^3/g	54%
D (H at $t_H = 30$ min)	25%	115 mm^3/g	48%
D (H at $t_H = 180$ min)	32%	174 mm^3/g	41%

Sulfur redistribution has been quantitatively assessed by means of CCSEM-EDX analysis (Figure 7 and Table 3). Similar to the spent sorbent, H samples show a bimodal distribution function. However, the core-zone area (Figure 2) decreases from 35% (spent sorbent) to 3% (sample steam-reactivated at $t_H = 180$ min), corresponding to a nearly uniform distribution of sulfur across the particle. Correspondingly, the variance of the distribution decreases from 216 (spent sorbent) to 70 ($t_H = 180$ min), further confirming the more even distribution of sulfur as t_H increases.

Dehydration (D) of reactivated sorbent

The following phenomena occur as H particles are reinjected in the hot fluidized bed: a) rapid heating up to the resulfation temperature (850°C); b) loss of steam due to the decomposition of $Ca(OH)_2$ to yield CaO (starting around 550°C). Both these phenomena are in turn responsible for particle fragmentation. The porous structure further developed by the dehydration of particles is mainly responsible for the subsequent SO_2 capture upon resulfation. These phenomena have been quantitatively assessed in dehydration (D) tests.

Figure 9 reports the particle size distribution of D particles. Dehydration brings about a noticeable fragmentation: 44% of the particles hydrated for $t_H = 180$ min fall in the size bin 0-0.4 mm after dehydration. This value decreases to 10-14% for samples hydrated at $t_H = 10$ and 30 min. More-

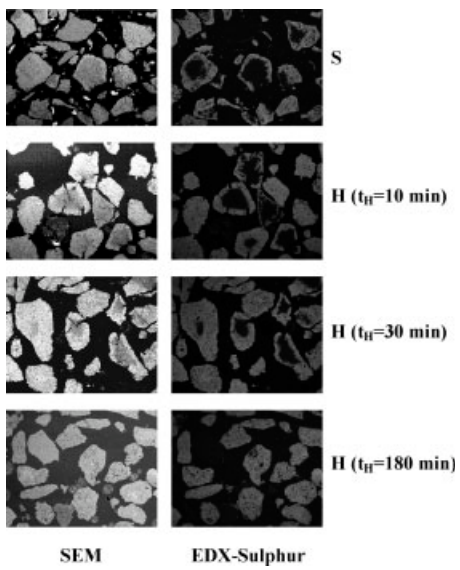

Figure 6. SEM-EDX analysis of cross-sections of S particles, and of H particles hydrated at t_H = 10, 30, and 180 min.

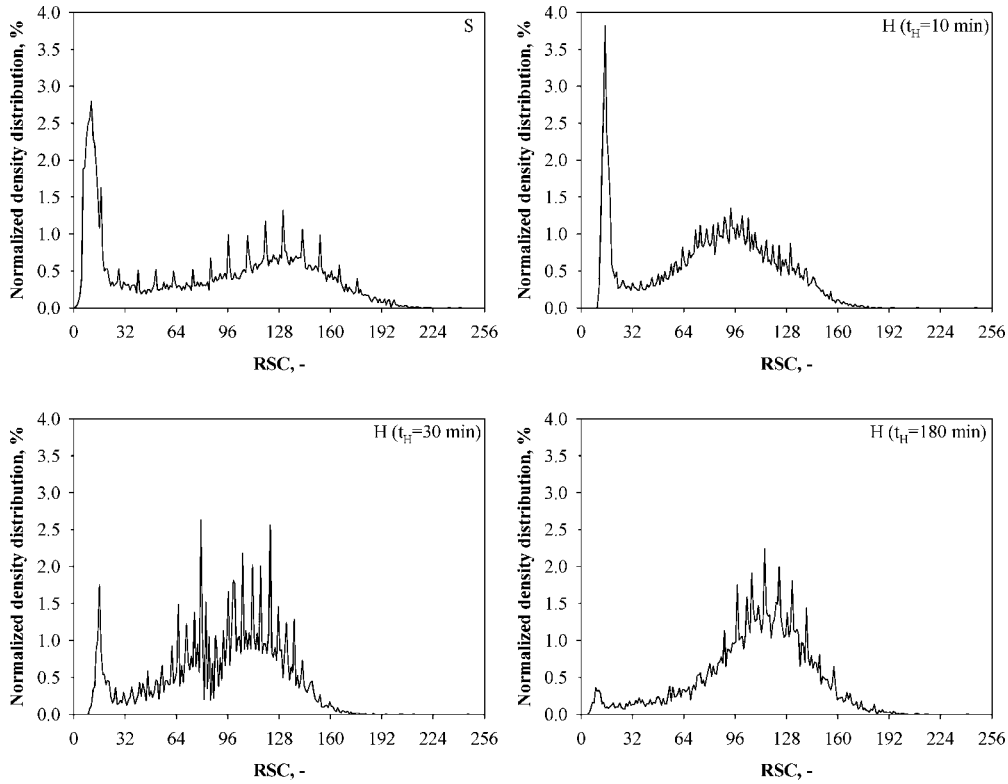

Figure 7. Probability density functions of Relative Sulfur Content (RSC) from CCSEM-EDX analysis of multiparticle samples.

over, the fractional mass of particles in the size range 0-0.1 mm is negligible after dehydration of particles hydrated for $t_H = 10$ and 30 min, while it is appreciable for the sample steam-hydrated for $t_H = 180$ min. The average Sauter diameters are 0.44, 0.42, and 0.27 mm for D samples hydrated at $t_H = 10$, 30, and 180 min, respectively. The extensive fragmentation of D samples deriving from long hydration times could obviously be related to the larger $Ca(OH)_2$ amount. On the one hand, larger portlandite contents give rise to more extensive steam release upon reinjection into the hot fluidized bed. On the other hand, it is likely that the more extensively hydrated samples are characterized by residual mechanical stresses associated with swelling of the unreacted core, which, in turn, might make them more susceptible to breakage upon impact or surface wear.

Results of the porosimetric characterization of D samples are summarized in Figure 5 and Table 2. Steam hydration/dehydration induces the development of accessible porosity. The longer t_H, the larger the accessible porosity: the cumulative specific pore volume (85 mm^3/g for the spent sorbent) is 102, 115, and 174 mm^3/g for the dehydrated sorbents hydrated at $t_H = 10$, 30, and 180 min, respectively. Correspondingly, the total porosities (19% for the spent sorbent) are 22%, 25%, and 32%. Apparently, the combined hydration/dehydration process affects the volume of the bigger pores to a larger extent than that of the finer pores.

Table 3. CCSEM-EDX Analysis Results for Multiparticle Samples

Sample	Core-Zone Area	Variance (σ^2)
S	35%	216
H ($t_H = 10$ min)	20%	143
H ($t_H = 30$ min)	10%	90
H ($t_H = 180$ min)	3%	70

Resulfation (RS) of reactivated sorbent

Figure 3 reports the calcium conversion degree $X_{Ca}(t)$ recorded during resulfation (RS) of reactivated sorbent samples. Reactivation effectively regenerates the sorption ability of the unsulfated calcium, as demonstrated by the further significant increase of X_{Ca} with respect to the value attained at the end of the first sulfation (28%). The ultimate calcium conversion degree increases as t_H increases: 36% when $t_H = 10$ min, 41% when $t_H = 30$ min, and 54% when $t_H = 180$ min.

Figure 4 reports the sorbent elutriation rate E(t) measured during resulfation tests. Sorbent samples hydrated for $t_H = 10$ and 30 min are characterized by a strong reduction of the elutriation rate with respect to that of the fresh sorbent. On the contrary, elutriation is far more extensive for the sorbent reactivated at $t_H = 180$ min. The attrition propensity can be satisfactorily correlated with the extent of sorbent hydration achieved during H tests. Regardless of the pre-treatment conditions, the sorbent elutriation rate decreases with sulfation time, as observed for the first sulfation of the raw sorbent, reflecting the parallel progress of particle rounding off and sulfation. Finally, it is recalled here that the impact of comminution phenomena on the sorbent performances should be considered in the light of two conflicting effects:

(i) elutriable fines generated by attrition/fragmentation are characterized by shorter residence times in the reactor

when compared with the parent particles, and this may negatively affect calcium conversion;

(ii) daughter fragments of smaller size are characterized by faster and more extensive calcium conversion when compared with the mother particles.

Whether and how the two effects balance each other cannot be established a priori, depending on the design and operational parameters of the FB process, and on the specific sorbent particle size distributions originating from attrition/fragmentation.

Conclusions

Steam hydration of a spent limestone sulfating according to the core-shell/network pattern is effective to regenerate the

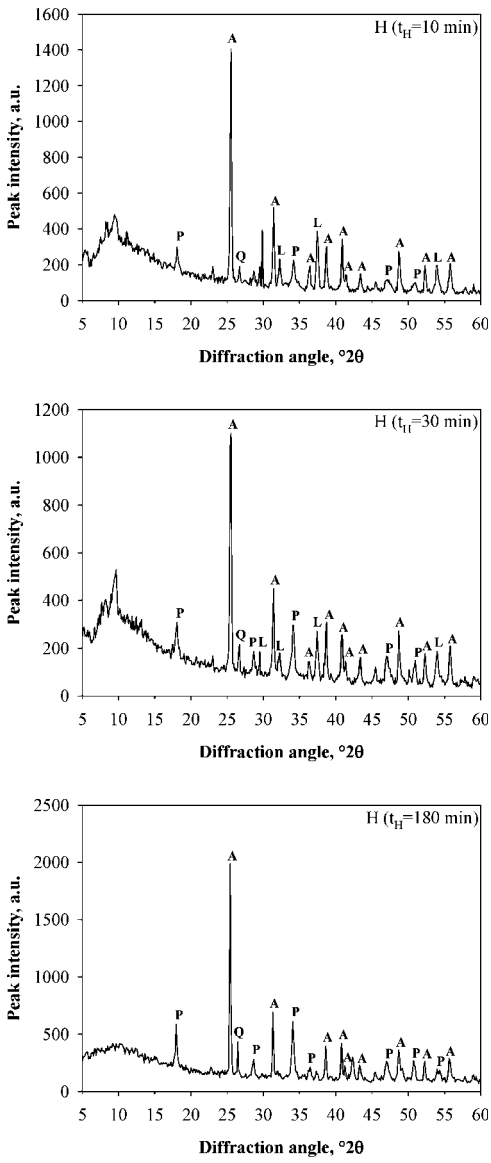

Figure 8. XRD spectra of H particles hydrated at t_H = 10, 30, and 180 min (A = anhydrite, $CaSO_4$; L = lime, CaO; P = portlandite, $Ca(OH)_2$; Q = quartz, SiO_2).

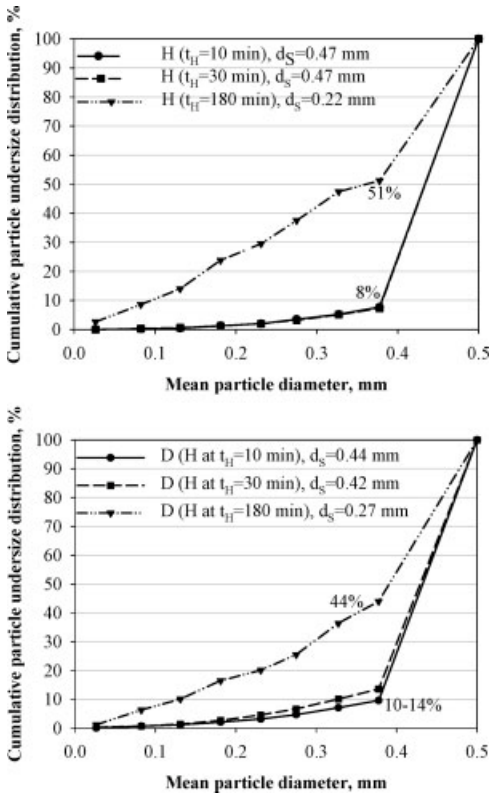

Figure 9. Cumulative particle undersize distribution of H and D samples.

SO_2 uptake ability of the sorbent: the degree of calcium utilization increases from 28% to 54% after a single exposure for 180 min at steam partial pressure of 0.05 MPa and at a temperature of 250°C. Samples collected after each step (sulfation of the raw sorbent, hydration and dehydration of the spent sorbent, and resulfation of the reactivated limestone) were separately characterized to clarify the key mechanisms of sorbent reactivation. Hydration of unreacted lime to $Ca(OH)_2$ is complete after 180 min under the hydration conditions tested. Lime hydration is responsible for the development of cracks and fissures within the sorbent particles, which enhances particle accessibility and further sulfur uptake. Hydrated samples are also characterized by a certain propensity to undergo fragmentation and attrition upon further processing in FB. Moreover, it is observed that hydration brings about a pronounced redistribution of sulfur across the particle cross-section; the non-uniform sulfur uptake typical of the core-shell and network sulfation patterns evens out, upon prolonged (180 min) hydration, into a remarkably uniform sulfur distribution. This process increases the availability of free lime in the particle outer layer, providing an additional pathway to the enhancement of sulfur capture. Dehydration of hydrated samples further contributes to opening up the porous structure. This affects both the accessibility of unreacted lime through the pore network as well as fragmentation and attrition of the regenerated sorbent particles.

Altogether, results of the present study suggest that a close correlation can be established among the change of textural and chemical characteristics induced by hydration/dehydra-

tion of spent sorbents, the regeneration of the spent sorbent sulfur uptake ability, and the attrition/fragmentation propensity of the reactivated sorbent particles. The assessment of the actual performance of the regenerated sorbent in the combustion chamber should take into account, on the one hand, the renewed hydration-induced sulfur uptake ability, and, on the other hand, the consequences that enhanced fragmentation and attrition of regenerated sorbent exert on particle size and residence time distribution.

Acknowledgments

The authors are grateful to Mr. Sabato Masi, Mr. Giuseppe Mocci, Mr. Sabato Russo, and Mrs. Clelia Zucchini for their valuable help in performing particle characterization.

Literature Cited

1. Lyngfelt A, Leckner B. SO_2 capture in fluidized-bed boilers: re-emission of SO_2 due to reduction of $CaSO_4$. *Chem Eng Sci*. 1989; 44:207–213.
2. Dennis JS, Hayhurst AN. Mechanism of the sulfation of calcined limestone particles in combustion gases. *Chem Eng Sci*. 1990;45:1175–1187.
3. Duo W, Laursen K, Lim J, Grace J. Crystallization and fracture: formation of product layers in sulfation of calcined limestone. *Powder Techn*. 2000;111:154–167.
4. Laursen K, Duo W, Grace JR, Lim J. Sulfation and reactivation characteristics of nine limestones. *Fuel*. 2000;79:153–163.
5. Anthony EJ, Granatstein DL. Sulfation phenomena in fluidized bed combustion systems. *Prog Energy Combustion Sci*. 2001;27:215–236.
6. Montagnaro F, Salatino P, Scala F. The influence of sorbent properties and reaction temperature on sorbent attrition, sulfur uptake, and particle sulfation pattern during fluidized-bed desulfurization. *Combus Sci Techn*. 2002;174(11–12):151–169.
7. Cheng J, Zhou J, Liu J, Zhou Z, Huang Z, Cao X, Zhao X, Cen K. Sulfur removal at high temperature during coal combustion in furnaces: a review. *Prog Energy Combustion Sci*. 2003;29:381–405.
8. Duo W, Laursen K, Lim J, Grace J. Crystallization and fracture: product layer diffusion in sulfation of calcined limestone. *Indus Eng Chem Res*. 2004;43:5653–5662.
9. Tarelho LAC, Matos MAA, Pereira FJMA. The influence of operational parameters on SO_2 removal by limestone during fluidised bed coal combustion. *Fuel Processing Techn*. 2005;86:1385–1401.
10. Scala F, Cammarota A, Chirone R, Salatino P. Comminution of limestone during batch fluidized-bed calcination and sulfation. *AIChE J*. 1997;43:363–373.
11. Scala F, Salatino P, Boerefijn R, Ghadiri M. Attrition of sorbents during fluidized bed calcination and sulfation. *Powder Techn*. 2000;107:153–167.
12. Chu CY, Hwang SJ. Attrition and sulfation of calcium sorbent and solids circulation rate in an internally circulating fluidized bed. *Powder Techn*. 2002;127:185–195.
13. Rozelle PL, Pisupati SV, Scaroni AW. Influence of petrographic composition of sorbents on attrition characteristics in a CFB boiler. *17th Int Fluidized Bed Combus Conf*. 2003: Paper No. 173.
14. Shimizu T, Peglow M, Yamagiwa K, Tanaka M. Comparison among attrition-reaction models of SO_2 capture by uncalcined limestone under pressurized fluidized bed combustion conditions. *Chem Eng Sci*. 2003;58:3053–3057.
15. Bernardo G, Marroccoli M, Montagnaro F, Valenti GL. Use of fluidized bed combustion wastes for the synthesis of low-energy cements. *11th Int Congress Chem Cement*. 2003;1227–1237.
16. Shearer JA, Smith GW, Moulton DS, Smyk EB, Myles KM, Swift WM, Johnson I. Hydration process for reactivating spent limestone and dolomite sorbents for reuse in fluidized-bed coal combustion. *6th Int Fluidized Bed Combus Conf*. 1980;1015–1027.
17. Couturier MF, Marquis DL, Steward FR, Volmerange Y. Reactivation of partially-sulfated limestone particles from a CFB combustor by hydration. *Can J Chem Eng*. 1994;72:91–97.
18. Julien S, Brereton CMH, Lim CJ, Grace JR, Chiu JH, Skowyra RS. Spent sorbent reactivation using steam. *13th Int Fluidized Bed Combus Conf*. 1995;841–849.
19. Scala F, Montagnaro F, Salatino P. Enhancement of sulfur uptake by hydration of spent limestone for fluidized-bed combustion application. *Indus Eng Chem Res*. 2001;40:2495–2501.
20. Davini P. Properties and reactivity of reactivated calcium-based sorbents. *Fuel*. 2002;81:763–770.
21. Laursen K, Mehrani P, Lim CJ, Grace JR. Steam reactivation of partially utilized limestone sulfur sorbents. *Environ Eng Sci*. 2003;20:11–20.
22. Laursen K, Duo W, Grace JR, Lim CJ. Cyclic steam reactivation of spent limestone. *Indus Eng Chem Res*. 2004;43:5715–5720.
23. Montagnaro F, Scala F, Salatino P. Reactivation by water hydration of spent sorbent for fluidized-bed combustion application: influence of hydration time. *Indus Eng Chem Res*. 2004;43:5692–5701.
24. Wu Y, Anthony EJ, Jia L. Steam hydration of CFBC ash and the effect of hydration conditions on reactivation. *Fuel*. 2004;83:1357–1370.
25. Wang J, Wu Y, Anthony EJ. The hydration behaviour of partially sulfated fluidized bed combustor sorbent. *Indus Eng Chem Res*. 2005; 44:8199–8204.
26. Scalari S, Grillo F, Salatino P, Pentolini M, Raggio G, Chirone R. Dynamic modelling of Enel Sulcis 790 MWth CFB combustion unit: model development and preliminary results. *19th Int Fluidized Bed Combus Conf*. 2006: Paper No. 89.
27. Montagnaro F, Salatino P, Scala F, Wu Y, Anthony EJ, Jia L. Assessment of sorbent reactivation by water hydration for fluidized bed combustion application. *J Energy Res Techn*. 2006;128: 90–98.
28. Wu Y, Anthony EJ, Jia L. Reactivation properties of four Canadian limestones. *19th Int Fluidized Bed Combus Conf*. 2006: Paper No. 10.
29. Montagnaro F, Salatino P, Scala F, Bernardo G, Valenti GL. Assessment of ettringite from hydrated FBC residues as a sorbent for fluidized bed desulfurization. *Fuel*. 2003;82:2299–2307.
30. Bernardo G, Telesca A, Valenti GL, Montagnaro F. Role of ettringite in the reuse of hydrated fly ash from fluidized-bed combustion as a sulfur sorbent: a hydration study. *Indus Eng Chem Res*. 2004;43:4054–4059.
31. Montagnaro F, Salatino P, Bernardo G, Telesca A, Valenti GL. Reuse of fly ash from a fluidized bed combustor for sulfur uptake: the role of ettringite in hydration-induced reactivation. *Energy & Fuels*. 2005;19:1822–1827.
32. Anthony EJ, McCleave R, Gandolfi E, Wang J. Industrial-scale demonstration of a new sorbent reactivation technology for fluidized bed combustors. *J Environ Management*. 2003;69:177–185.
33. Montagnaro F. Characterization of sulfation and of hydration-induced reactivation of sorbents in fluidized bed systems. Ph.D. Thesis in Chemical Engineering, University of Naples Federico II, 2003.
34. Dam-Johansen K, Østergaard K. High-temperature reaction between sulfur dioxide and limestone—I. Comparison of limestones in two laboratory reactors and a pilot plant. *Chem Eng Sci*. 1991;46:827–837.
35. Dam-Johansen K, Østergaard K. High-temperature reaction between sulfur dioxide and limestone—II. An improved experimental basis for a mathematical model. *Chem Eng Sci*. 1991;46:839–845.

Manuscript received Jan. 13, 2006, and revision received Sept. 12, 2006.